



Research papers

Scaling of precipitation extremes with temperature in China's mainland: Evaluation of satellite precipitation data

Seyed-Mohammad Hosseini-Moghari^a, Siao Sun^b, Qihong Tang^{a,c,*}, Pavel Yakovlevich Groisman^{d,e,f}

^a Key Laboratory of Water Cycle and Related Land Surface Processes, Institute of Geographic Sciences and Natural Resources Research, Chinese Academy of Sciences, Beijing 100101, China

^b Key Laboratory of Regional Sustainable Development Modeling, Institute of Geographic Sciences and Natural Resources Research, Chinese Academy of Sciences, Beijing 100101, China

^c University of Chinese Academy of Sciences, Beijing 100049, China

^d North Carolina State University at NOAA National Centers for Environment Information, Asheville, USA

^e P.P. Shirshov Institute for Oceanology, RAS, Moscow, Russia

^f Hydrology Science and Services Corp, Asheville, USA



ARTICLE INFO

Keywords:

Clausius–Clapeyron
Dew point temperature
IMERG
Peak structure
Scaling factor
Surface air temperature

ABSTRACT

This study explores the sensitivity (termed scaling factor, SF) of daily and 30-minute precipitation extremes with several temperature variables, i.e., within-day surface air temperature (SAT) and dew point temperature (DPT), and antecedent SAT and DPT (corresponding to temperatures one day before a precipitation event, denoted as SAT-C and DPT-C) across China's mainland. To this end, we used observed daily meteorological data from CN05.1 dataset and 30-minute precipitation data from the Integrated Multisatellite Retrievals for the Global Precipitation Measurement (IMERG). Our results reveal a mix of the positive and negative SFs of extreme daily precipitation with SAT across climatic zones, with peak-like structures developing at higher temperatures (between 17 and 24 °C). Although almost all the SFs turn to positive when SAT-C, DPT, and DPT-C are used, a peak structure is observed over some parts of each climate zone, especially in tropical regions. A comparison between the SFs of the full temperature range and the temperature range before peak structure reveals that a single scaling rate is not valid for the entire temperature range. Moreover, the SFs calculated based on the temperature range before the peak structure (for all four types of temperatures) follow better the Clausius–Clapeyron scaling (~7%/°C) than the SFs of the full temperature range except for the tropical region. Daily SFs based on IMERG data are mostly comparable to CN05.1 results, with discrepancies mainly in tropical and plateau climates (roughly 25% of the study area). However, IMERG's 30-min precipitation extremes do not rise as much as expected (even decrease in some parts of the country) with increasing temperatures, contrary to common observations reported in previous studies. It suggests that another precipitation dataset is needed for scaling precipitation extremes at a 30-minute scale, at least for China's mainland.

1. Introduction

Substantial evidence suggests that in the presence of sufficient atmospheric water vapor supply, heavier precipitation is likely to occur at higher temperatures (Hegerl et al., 2015; Schroeer and Kirchengast, 2018; Tang, 2020). Indeed, based on the Clausius–Clapeyron (CC) relation, the atmosphere's moisture-holding capacity increases by ~7% per °C of warming (Held and Soden, 2006; Trenberth et al., 2003). As a

result, the precipitation intensity is expected to increase as temperature rises (Berg et al., 2009; Gao et al., 2020). Understanding the relationship between extreme precipitation and temperature is a crucial step towards grasping how precipitation intensity will change under future global warming (Bui et al., 2019). Although the rate of changes in extreme precipitation with increasing temperature is not constant for different storm types and durations. However, having different scenarios about future changes in extreme precipitation could help us to better estimate

* Corresponding author at: Key Laboratory of Water Cycle and Related Land Surface Processes, Institute of Geographic Sciences and Natural Resources Research, Chinese Academy of Sciences, Beijing 100101, China.

E-mail address: tangqh@igsnr.ac.cn (Q. Tang).

<https://doi.org/10.1016/j.jhydrol.2021.127391>

Received 23 June 2021; Received in revised form 24 November 2021; Accepted 21 December 2021

Available online 28 December 2021

0022-1694/© 2021 Elsevier B.V. All rights reserved.

the design of hydrological extremes in a warming climate as discussed in Sharma et al. (2021). To address this issue, the sensitivity of precipitation to temperature (the rate of increase in precipitation intensity with one degree of warming, termed scaling factor (SF)), has been analysed over many regions, such as Australia (Hardwick Jones et al., 2010; Herath et al., 2018; Wasko and Sharma, 2015), France (Drobinski et al., 2016), India (Ali and Mishra, 2017), Japan (Fujibe, 2013; Utsumi et al., 2011), Poland (Wibig and Piotrowski, 2018), the United States (Barbero et al., 2017; Mishra et al., 2012), and United Kingdom (Blenkinsop et al., 2015; Chen and Li, 2016).

However, there are two main barriers to the calculation and interpretation of the SF. The first barrier in some regions, particularly at low latitudes, is negative SF values observed in the relationship between extreme daily and sub-daily precipitations and the surface air temperature (SAT). There is a peak structure in the precipitation-temperature relation; that is, extreme precipitation increases at the low-medium range of SAT but decreases at high SAT. This reduces the robustness of using SF in estimating extreme daily and sub-daily precipitation changes in a warming climate (Sun et al., 2020; Zhang et al., 2017). The reasons for the occurrence of a peak structure in the daily or sub-daily precipitation-temperature curve include limitations in moisture availability at high SAT (Hardwick Jones et al., 2010), the intra-seasonal variation of temperature (Berg et al., 2009), decreasing wet time fraction (Utsumi et al., 2011; Visser et al., 2021) and increasing short convective thunderstorms at high SAT (Westra et al., 2014), the cooling effect after precipitation (Ali and Mishra, 2017), and solar radiation blocking by heavy cloudiness (Escrig et al., 2013).

To deal with the first barrier, a few studies calculated SFs separately for each season, storm duration, or storm type and found that their results are more consistent with the CC relation compared to when the whole data were considered together (e.g., Berg et al., 2009, 2013; Panthou et al., 2014). Some others suggested using dew point temperature (DPT) instead of SAT as an alternative temperature variable (e.g., Ali & Mishra, 2017; Bui et al., 2019; Wasko et al., 2018). By far, the use of DPT provides closer results to our expectation from CC relation because DPT takes into account both temperature and moisture availability at the land surface, and SF based on DPT may not be as sensitive to storm duration (Wasko et al., 2018) and precipitation type (Bui et al., 2019). On a global scale, Ali et al. (2018) and Zhang et al. (2019) showed that the results of DPT in scaling extreme daily precipitation are more consistent with the expected CC relation compared to SAT. Similar results were reported for scaling the extreme daily and sub-daily precipitation in India (Ali and Mishra, 2017), the Netherlands (Lenderink et al., 2011), France (Drobinski et al., 2016), western Europe (Lenderink and Van Meijgaard, 2010), Canada (Panthou et al., 2014), and Australia (Wasko et al., 2018). Although positive SF values were reported for the extreme precipitation-DPT relationship, some studies concluded that the peak structure still remains, e.g., over the Netherlands (Zhang et al., 2017) and South Korea (Park and Min, 2017). More recently, Visser et al. (2020) showed that using the antecedent dry-bulb temperature (antecedent temperature represents temperature before a precipitation event) can address cooling effects on scaling the peak hourly precipitation and result in positive SFs across a wide range of climatic regions. However, it is not clear whether applying antecedent temperature is useful in addressing the peak structure and then a single scaling rate can be appropriately applied at higher temperatures.

The second barrier is the limitation of the data, practically at a sub-daily scale. In many parts of the world, we do not have enough precipitation data with a fine spatial-temporal resolution, e.g., sub-daily precipitation (Trenberth et al., 2017), to build a meaningful relationship between precipitation extremes and temperatures. Lewis et al. (2019) tried to break through this barrier by developing a Global Sub-Daily Rainfall Dataset (GSDR). This quality-controlled dataset is becoming one of the primary sources of observed sub-daily precipitation data. So far, several studies have shown the usefulness of this dataset at an hourly scale (e.g., Ali et al., 2021; Barbero et al., 2019; Li et al.,

2020). However, this dataset does not cover the whole globe (it covers only some parts of the land) and is not accessible to the public due to the restriction policy. Fowler et al. (2021) stated that we should be aware of the strengths and weaknesses of using remotely sensed precipitation datasets as an alternative source to analyse the precipitation-temperature relationship. Although remotely sensed precipitation datasets often suffer low accuracy in comparison to gauge measurements, they are a potential alternative source to analyse the perception-temperature scaling at a sub-daily scale due to their high spatiotemporal resolution, global spatial coverage, and considerable temporal span. Therefore, the evaluation of using satellite-based precipitation datasets in scaling precipitation with a temperature is a real need. In this regard, Wasko et al. (2016) presented a quasi-global assessment of the Tropical Rainfall Monitoring Mission (TRMM) 3B4 for scaling precipitation extremes at 3-hourly and daily time scale. They found that the performance of TRMM is significantly varied in different regions and time scales; however, its data can be used in ungauged areas. Among different remotely sensed precipitation products, the Integrated Multisatellite Retrievals for the Global Precipitation Measurement (IMERG) as the most current satellite-based precipitation dataset might be a valuable option because 1) the IMERG provides global 30-minute precipitation intensity, 2) the data are accessible to all the researchers without any restrictions (Hosseini-Moghari and Tang, 2020).

Three questions remain open for investigation: 1) What is the effect of antecedent temperature on the peak structure, 2) Is a single scaling rate valid across the temperature ranges? and 3) Can the remotely sensed precipitation data be a reliable alternative to in-situ precipitation? To address the first question, we investigate extreme precipitation changes with within-day SAT and DPT as well as antecedent SAT/DPT. The antecedent SAT/DPT can be a better proxy than SAT/DPT, particularly over tropical regions. The antecedent temperature could potentially reflect the actual temperature attributed to the precipitation event without being affected by the cooling impact of precipitation events and heavy cloud cover that accompanies these events. It should be noted that there are already several studies that investigated the relationship between daily and sub-daily precipitation extremes and temperatures over China, e.g., Gao et al. (2020), Wang et al. (2018), Guo et al. (2020), and Yong et al. (2021). However, in this study, our focus is on the spatial variation of the peak structure based on four types of temperature and the capability of the satellite precipitation product to capture the peak structure. To deal with the second question, we compare SFs calculated based on temperature range prior to peak structure with SFs for the full temperature range to see how SF rates change across the temperature ranges. We address the third question in two steps owing to limitations in the observed data. Firstly, we use the gauge-based dataset to quantitatively evaluate the IMERG's performance in scaling daily precipitation extremes with temperatures. Later, we use precipitation data from the IMERG for scaling 30-minute precipitation extremes with temperatures over China's mainland and compare the results with previous studies and the CC relation. The remainder of this paper is organized as follows: study area and data are described in Section 2. Sections 3, 4, and 5 show the study's method, results, and discussion, respectively. Finally, conclusions are drawn in Section 6.

2. Study area and data

We focus on scaling precipitation extremes with temperature variables in China's mainland. With a population of ~ 1.4 billion people (Li et al., 2019), China is the world's most populous country. Natural disasters, especially floods and landslides driven by extreme rainfall events, cause high economic and social losses in this country (Han et al., 2016). It is estimated that one degree of warming will result in more than US\$130 billion flood loss per year throughout the nation (Jiang et al., 2020). Therefore, understanding the extreme precipitation changes with temperature in China is the key to manage these disasters under future global warming. We used the daily climate dataset CN05.1

provided by the National Climate Center of China Meteorological Administration (Wu and Gao, 2013). CN05.1 is a gridded $0.25^\circ \times 0.25^\circ$ dataset based on a dense network of 2416 in-situ weather stations provided by the Chinese Meteorological Administration (Yang et al., 2017). CN05.1 provides daily meteorological data for the period 1961–2017. We obtained the daily precipitation, SAT, and relative humidity from CN05.1. The DPT was calculated based on SAT and relative humidity using the Magnus-Tetens formula (Barenbrug, 1974).

In addition to CN05.1 data, we utilized the IMERG version 6 final run precipitation product at daily and 30-minute timescales. The IMERG data with a $0.1^\circ \times 0.1^\circ$ spatial resolution are available from June 2000 onwards over the entire globe (Caloiero et al., 2021). Additional information about the IMERG product can be found in Huffman et al. (2015). We considered a common period to compare IMERG with CN05.1 at the daily scale, i.e., 2000 to 2017. At a 30-minute scale, storm events are identified using a two-hour separator, i.e., two precipitation events are considered independent if they are separated by two consecutive hours of zero precipitation (see Wasko and Sharma, 2015). Then, we considered the maximum 30-minute intensity in each independent storm to calculate SF at the 30-minute scale. Since the SF is usually dependent on climatic zones (Panthou et al., 2014), we considered the Köppen-Geiger climate classification (Köppen, 1936; Peel et al., 2007) and classified China's mainland into five climatic zones (see Fig. S1, i.e., arid (northwest), continental (northeast), plateau climate (Tibetan Plateau), humid (southeast), and tropical (south islands) according to the climate classification map from Beck et al. (2018).

3. Method

To calculate SF, we applied the binning technique with an equal number of events per bin because of its better performance over the approach with equal width temperature bins. Indeed, applying the binning approach with equal width may lead to fewer pairs in bins at the lower and upper ends and, in some cases, may result in empty bins, which would distort the extreme precipitation-temperature relationship (Herath et al., 2018). At daily scale, similar to previous studies in China (e.g., Yin et al., 2021; Yong et al., 2021), the precipitation events higher than 0.1 mm/day were grouped with corresponding daily temperatures to apply this technique for each pixel. We considered within-day SAT/DPT and antecedent SAT/DPT (from here onwards referred to as SAT-C/DPT-C) to offset the surface cooling effect during the rainfall. Then the precipitation-temperature pairs were sorted in ascending order by temperature. The pairs were placed into 12 bins with an equal number of pairs per bin. If the bins for a given pixel contained less than 101 pairs, we omitted that pixel from the calculation, i.e., only those pixels with at least 1212 events (12 bins and more than 100 pairs in each bin) were considered in the calculation. We then estimated the 99th percentile daily precipitation (P99, to represent precipitation extreme) and mean SAT/DPT/SAT-C/DPT-C (\bar{T}) for each bin. Finally, we fitted the following linear regression (Ali et al., 2018; Ali and Mishra, 2017; Bui et al., 2019) to the P99 and mean SAT/DPT/SAT-C/DPT-C data for each pixel:

$$\ln(\text{P99}) = \beta_1 \bar{T} + \beta_0 \quad (1)$$

where β_1 and β_0 are slope and intercept of the linear regression, respectively. Eventually, the SF was estimated for each pixel by (Bui et al., 2019):

$$\text{SF}(\% / ^\circ\text{C}) = (e^{\beta_1} - 1) \times 100 \quad (2)$$

SF was also calculated based on the median of SAT/DPT/SAT-C/DPT-C data in the bins with equal width. The results were comparable. Therefore, we only present the results based on mean daily SAT/DPT/SAT-C/DPT-C.

A similar process was applied for the 30-minute scale. Recall that, unlike the daily scale in which we considered all precipitation values larger than 0.1 mm/day, in calculating scaling factor at a 30-minute

scale, we use the maximum 30-minute intensity of each independent event with intensity larger than 0.1 mm/hr. In this way, the events with a long duration do not have more weight on the scaling rate than other events.

To identify a peak structure in the relationship between precipitation and temperature, we calculated the difference between the precipitation intensity in the bin with the highest temperature and the maximum precipitation intensity of all the bins. A zero difference indicates no peak structure. Therefore, we considered the following two equations to examine the peak structure in the precipitation-temperature relationship:

$$\Delta P(\%) = \frac{P99_m - P99_h}{P99_m} \times 100 \quad (3)$$

$$\Delta T(^{\circ}\text{C}) = T_{P99_m} - T_{P99_h} \quad (4)$$

where ΔP indicates the relative difference between the maximum of the 99th percentile of precipitation and the 99th percentile of precipitation in the bin with the highest temperature, ΔT (Δ SAT, Δ DPT, Δ SAT-C or Δ DPT-C) is the difference between the 99th percentile temperature in the bin corresponding to maximum precipitation intensity and 99th percentile temperature in the bin with the highest temperature, $P99_m$ and $P99_h$ represent maximum of the 99th percentile precipitation of all the bins and 99th percentile precipitation in the bin with the highest temperature, respectively; T_{P99_m} and T_{P99_h} are the temperatures corresponding to the $P99_m$ and $P99_h$, respectively.

As discussed in Visser et al. (2021), the binning technique provides a unique opportunity to analyze precipitation changes within a given temperature range. To take advantage of this feature, we calculated SF for the entire temperature range and the temperature range before the peak structure to examine peak structure impact on SF rates. To avoid calculating SF based on a limited number of data, we calculated SFs only for pixels with more than 1212 events (12 bins and more than 100 pairs in each bin) before T_{P99_m} .

4. Results

4.1. Scaling observed daily precipitation extremes with temperatures

Fig. 1 shows the spatial distribution of SFs based on SAT, DPT, SAT-C, and DPT-C in different climate zones of China's mainland. With respect to the t -test at a confidence level of 95 %, a statistically significant relationship between precipitation and SAT is found in 53.7 % of pixels. This value reaches 98.5, 93.7, and 92.8 % when DPT, SAT-C, and DPT-C are used. A negative SF based on SAT is found in regions of all climate zones except the continental climate zone (Fig. 1a). Overall, a negative SF between precipitation and SAT is present in 18.2 % of areas, concentrated in humid and tropical, whereas SF values based on DPT are always positive (Fig. 1b). Using SAT-C and DPT-C, the SFs are positive near everywhere over all zones; however, the SF values based on DPT are higher than the others. The biggest difference can be observed in tropical regions where SF-SAT varies between -5.6 and $+5.1$ %/ $^{\circ}\text{C}$, while an above CC-like scaling is obtained for all pixels based on DPT, SAT-C, and DPT-C. In more than half of the study area, SF values based on DPT are not lower than CC. Conversely, based on SAT, SAT-C, and DPT-C, more than 81, 69, and 80 % of areas have a SF value less than CC, respectively. Using SAT-C and DPT-C lead to lower SF values than using DPT; however, the SF values are always positive based on SAT-C and DPT-C.

Fig. 2 illustrates the density scatter plots of extreme daily precipitation versus different temperatures for each climate zone. A regression line was fitted between the 99th percentiles of precipitations and corresponding temperatures. From Fig. 2, a peak structure is observed in the relationship between SAT and precipitation, except for the plateau climate. This hook-shape relationship expresses a changing scaling from positive to negative, occurs in SAT ranges from 17 to 24 $^{\circ}\text{C}$ across China.

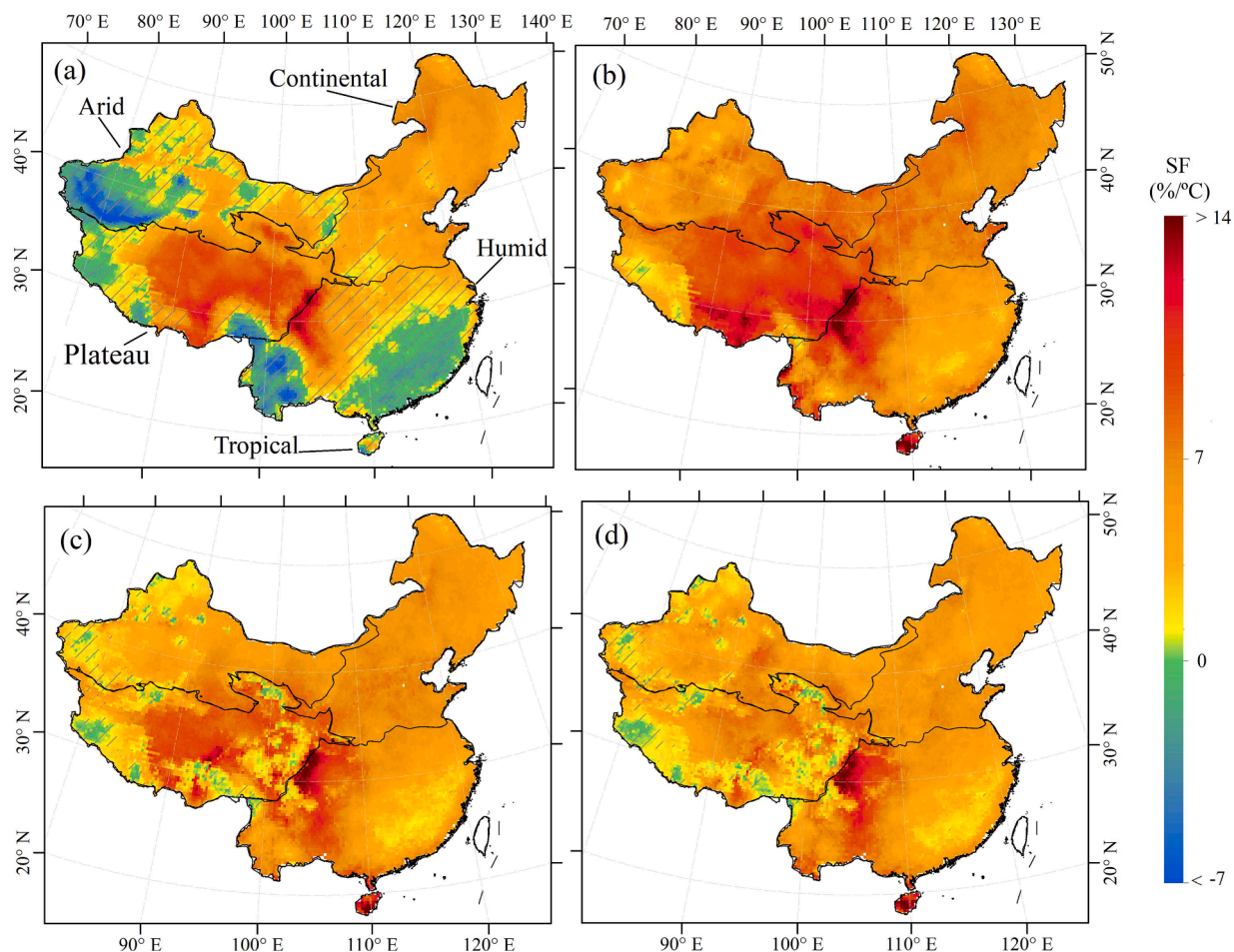


Fig. 1. Spatial distribution of SFs for 99th percentile of daily precipitation of CN05.1 in relation with (a) SAT, (b) DPT, (c) SAT-C, and (d) DPT-C over China's mainland. The polygons outlined by black lines represent five major climate zones in China's mainland. The gray diagonal lines represent the regions without a statistically significant relationship between extreme precipitation and SAT/DPT/SAT-C/DPT-C at the 95% confidence level based on the *t*-test. SF greater than 14 %/°C was set as 14 %/°C.

The use of DPT leads to an absence of the peak structure over the arid and continental areas, while the peak remains with a smoother slope over the humid and tropical regions. As a result, a high positive SF value (see Fig. 1) refers only to the curve's rising limb and is not necessarily linked to an absence of peak structure. When SAT-C is used, the results are almost similar to DPT; however, SAT-C leads to an almost flat curve at higher temperatures in the humid and tropical regions. Generally, there is no clear peak in the relationship between precipitation and DPT-C, suggesting that DPT-C results are more consistent with our expectation from CC relation. It should be noted that Fig. 2 shows a general behavior over each climate zone which means that it is possible for some pixels not to contribute to the tails of the scatter plots due to their limited temperature range. To deal with this issue, a pixel-by-pixel analysis is done below.

Fig. 3 shows box plots of ΔP and ΔT (see equations (3) and (4)) for five major climate zones. The median of ΔP based on SAT varies from 39 % (in the plateau region) to 87 % (in the tropical region). Thus, the extreme precipitation of the hottest bin in tropical region is much lower than the maximum extreme precipitation. Similarly, ΔT shows large variability with the median between -9.3 °C (in arid region) and -4.3 °C (in tropical region). Results indicate that the use of other temperature variables reduces ΔP and ΔT . In more than 70, 67, 50 % of areas of arid, continental, and plateau regions, ΔP and ΔT based on DPT are equal to zero. In humid and tropical regions, ΔP and ΔT are never equal to zero. SAT-C results are less consistent with the CC scaling than DPT in arid, continental, and plateau areas, whereas the opposite is true

in humid and tropical areas. Results based on DPT-C show smaller ΔP or ΔT in humid and tropical regions (with a median of ΔP equal to 10 % and 18 % and a median of ΔT equal to -2.4 °C and -1.5 °C in humid and tropical regions, respectively), suggesting that SFs based on DPT-C follow a better CC relation in these regions. The spatial pattern of ΔP and ΔT are presented in Figs. S2 and S3.

Fig. 4 illustrates box plots of SFs calculated based on the whole temperature range and the temperature range before the peak structure in five major climate zones (see Method section). Comparing two panels of Fig. 4 reveals that SFs before the peak point are stronger than SFs of full temperature range, particularly when SAT is used. SFs based on SAT are equal and bigger than SFs of other temperatures when the temperature range is limited to before the peak structure. It means that a single SF not only can be quite different based on different temperatures (Fig. 1), but also it varies significantly in different temperature ranges based on a given type of temperature (Fig. 4). The medians of the SF values of full temperature range based on SAT (DPT, SAT-C, DPT-C) in the arid, continental, plateau, humid, and tropical climate zones are 1.9 (6.3, 3.9, 4.1), 4.8 (6.4, 5.4, 4.9), 6.6 (8.7, 5.5, 3.9), 1.3 (5.2, 5.1, 4.9), and 0.6 (12.2, 11.3, 12.0) %/°C, respectively. While the medians of SF values reach to 7.1 (7.4, 4.4, 4.7), 6.6 (6.7, 5.5, 4.9), 9.9 (9.0, 7.4, 5.1), 6.2 (6.2, 5.6, 5.3), and 22.0 (16.4, 17.1, 13.0) for the arid, continental, plateau, humid, and tropical climate zones, respectively; for temperatures range before the peak structure. It shows that SFs before the peak structure are more consistent with the expected CC relation in the arid, continental, plateau, and humid regions than SFs computed based on the

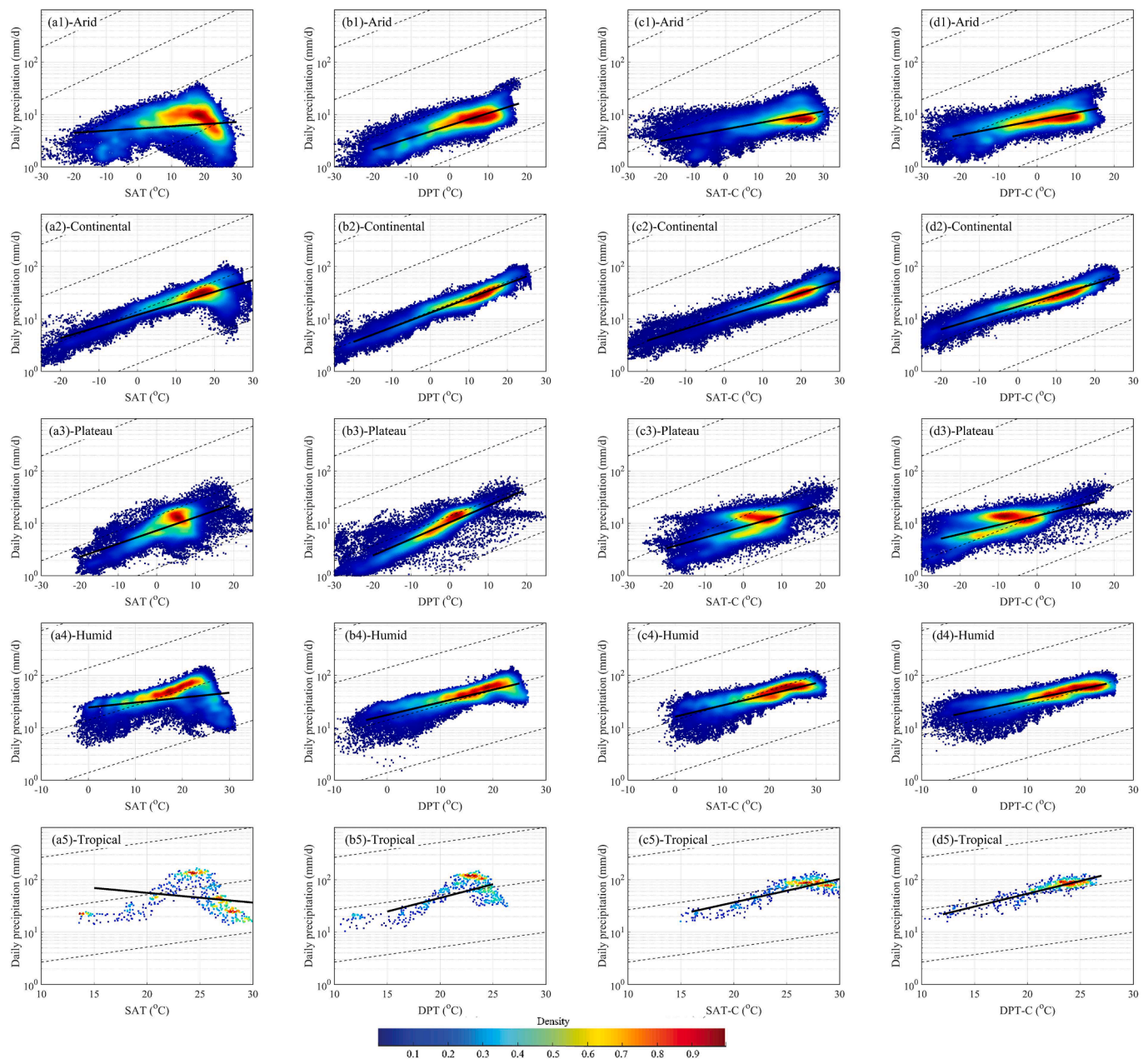


Fig. 2. The relationship between 99th percentile of daily precipitation and (a) SAT, (b) DPT, (c) SAT-C, and (d) DPT-C in (1) arid, (2) continental, (3) plateau, (4) humid, and (5) tropical climate zones of China. The solid black lines represent the 99th percentile lines fitted between extreme daily precipitation and corresponding SAT/DPT/SAT-C/DPT-C. The dashed black lines indicate CC like scaling of 6.8%/°C. Shaded colors indicate the probability density of the data based on a Gaussian kernel estimator. The y-axis has a logarithmic scale.

full temperature range.

4.2. Scaling daily precipitation extremes with temperatures using the IMERG data

Fig. 5 displays the box plots of SFs in different climate zones obtained from the observed and IMERG daily precipitation. Recall that the SFs in this section were computed for 2000–2017 (the common period in the observed and IMERG datasets). Generally, IMERG can reflect the impacts of different temperatures on SFs. IMERG based SF values are close to CN05.1 results except over the plateau and tropical areas. Larger SF values over plateau (generally above CC-like scaling) and lower SF values in tropical region (generally below CC-like scaling) are found from IMERG results compared to observed ones. A comparison between the results of different precipitation datasets and different temperatures

reveals SFs are more sensitive to the temperature variable than precipitation datasets at the daily scale. In other words, accurate sampling has a great impact on SF rates. For example, in the arid region, the difference between average SFs obtained from different temperatures varies from 0.04 (a difference when SAT-C and DPT-C are used) to 4.81 (a difference when SAT and DPT are applied); while the difference between CN05.1 and IMERG varies from 0.09 (when DPT-C is applied) to 2.55 (when SAT is used).

The spatial distribution of the difference between calculated SFs based on IMERG and CN05.1 using different temperature variables is shown in Fig. 6. It should be noted that in some pixels, there were not a sufficient number of precipitation events to calculate SF during 2000–2017 (less than 1212 events, see Method section). Indeed, about 50 % of the arid region and 16 % of the plateau region were excluded from the calculations. From Fig. 6, the difference between IMERG and

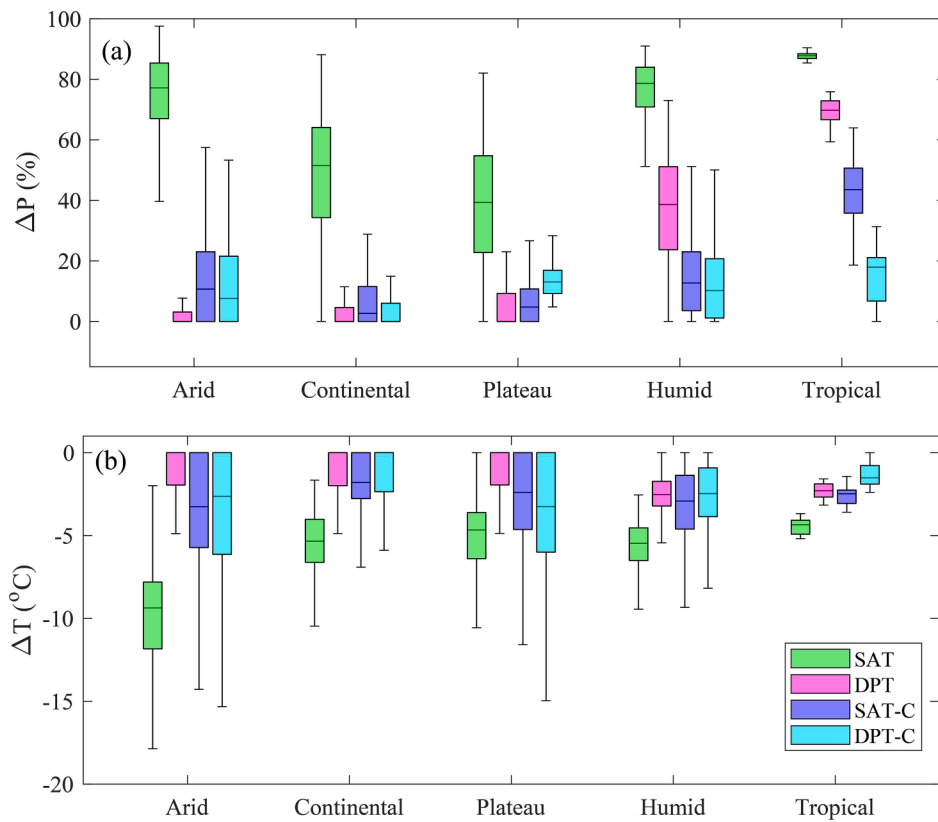


Fig. 3. Box plots of (a) ΔP and (b) ΔT for five major climate zones of China's mainland. ΔP indicates the relative difference between the maximum extreme precipitation within the bins and extreme precipitation in the bin with the highest temperature. ΔT shows the difference between temperatures in the bin with maximum extreme precipitation and the hottest bin. The bottom, middle, and top lines of each box are the 25th, 50th and 75th percentiles of the difference, respectively, and whiskers are the 5th and 95th percentiles of the difference, respectively.

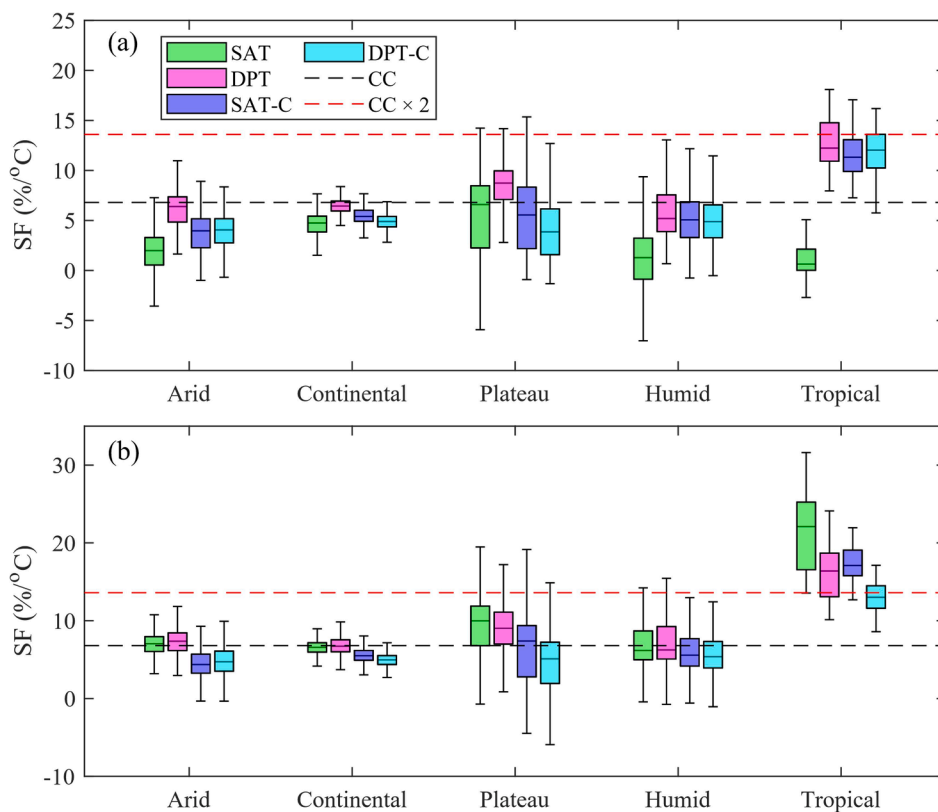


Fig. 4. SFs for (a) the entire temperature range and (b) the temperature range prior to peak structure in five major climate zones of China's mainland. The bottom, middle, and top lines of each box are the 25th, 50th and 75th percentiles of SF, respectively, and whiskers are the 5th and 95th percentiles of SF. The dashed black and red lines indicate CC and super CC like scaling of 6.8 and 13.6 %/°C, respectively (For interpretation of the references to colour in this figure legend, the reader is referred to the web version of this article.)

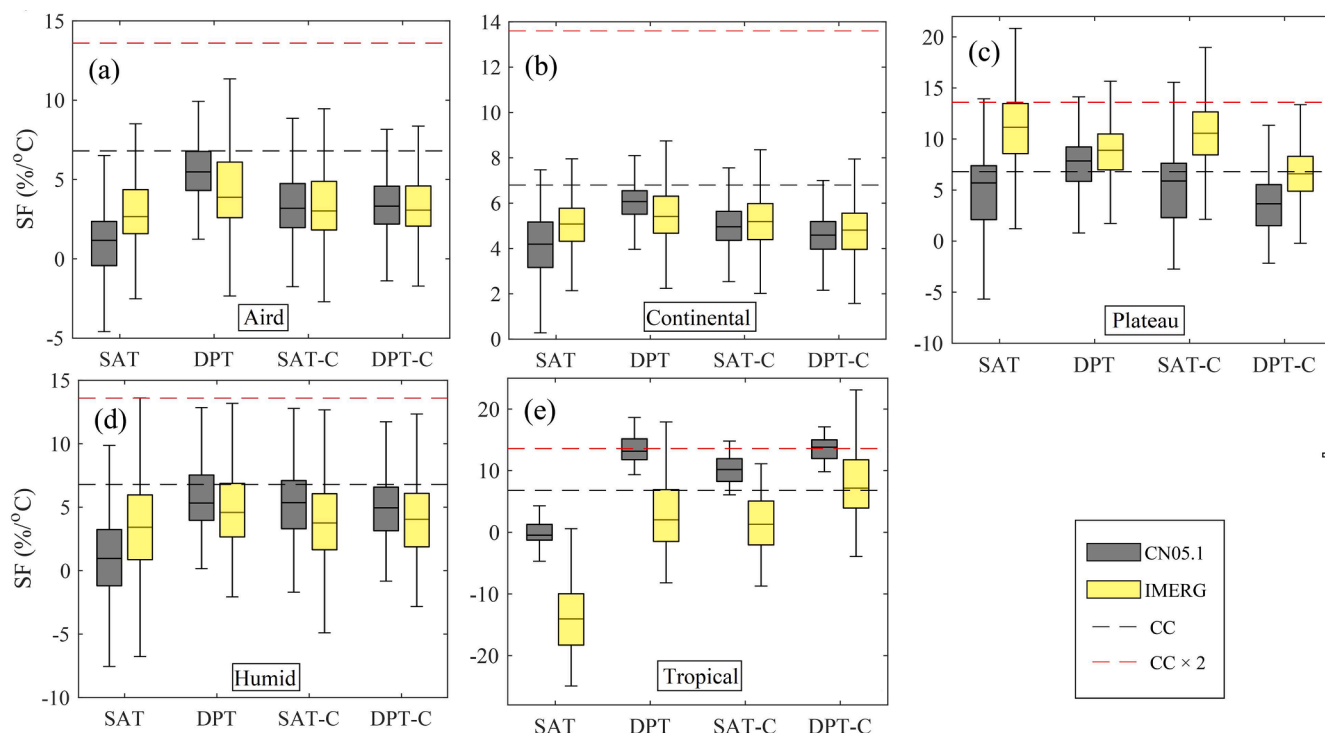


Fig. 5. Comparison between SFs for 99th percentile of daily precipitation of CN05.1 (grey) and IMERG (yellow) using SAT, DPT, SAT-C, and DPT-C for in (a) arid, (b) continental, (c) plateau, (d) humid, and (e) tropical climate zones of China's mainland. The bottom, middle, and top lines of each box are the 25th, 50th and 75th percentiles of SF, respectively, and whiskers are the 5th and 95th percentiles of SF. The dashed black and red lines indicate CC and super CC like scaling of 6.8 and 13.6 %/°C, respectively. (For interpretation of the references to colour in this figure legend, the reader is referred to the web version of this article.)

CN05.1 results is close to zero over a large part of China's mainland, particularly when DPT or DPT-C are used. The best results were found over continental and arid areas. The poorer performance of IMERG over the plateau and south parts compared to other regions can be explained by the complexity of precipitation estimation over these areas.

To compare extreme precipitation-temperature curves based on observed and IMERG datasets, a regression line was fitted between the 99th percentiles of daily precipitations and corresponding temperatures (the density scatter plots of IMERG extreme daily precipitation versus different temperatures are placed in the supplementary i.e., Fig. S4. Fig. 7 indicates that in many areas, the curves from CN05.1 and IMERG show similar patterns. In general, IMERG performs better at the medium temperature range than the tails of the curve. The main differences come from the amount of precipitation; somehow, the curves related to IMERG are generally located above CN05.1 ones. It means that the IMERG estimates more precipitation than is reported by observations.

Interestingly, IMERG can represent the impact of different temperatures on the peak structure well and, in most cases, shows a quite similar behavior compared to CN05.1. For example, the peak structure occurs around 23 °C in the tropical area based on both CN05.1 and IMERG data sets when SAT and DPT are used.

4.3. Scaling 30-minute precipitation extremes with temperatures based on IMERG

Fig. 8 shows the spatial pattern of SFs based on different temperatures at the 30-minute scale along with the box-plot of SFs over different climate zones. Unlike the daily scale, the areas with an insignificant relationship between the 30-minute extreme precipitation and temperature are considerable when DPT, SAT-C, and DPT-C are used. With respect to the *t*-test, there is no significant relationship between precipitation and SAT (DPT, SAT-C, DPT-C) in 39.5% (33.5%, 38%, 33%) areas of China's mainland, mainly over arid and plateau regions. Moreover, SF values are smaller than the daily scale ones, and the

influence of different temperatures is negligible compared to its influence on the daily scale (compare Figs. 1 and 8). The largest impact of different temperatures can be seen over tropical lands, where the mean of SF values calculated based on DPT and DPT-C are at least twice larger than the values obtained from SAT and SAT-C. The median of SF values varies between [0.63, 1.35], [3.44, 3.50], [3.34, 4.21], [3.22, 3.78], [−8.81, −2.57] based on different temperatures in arid, continental, plateau, humid, and tropical climate zones, respectively.

The negative SFs over tropical land based on all temperatures and a below CC scaling in other parts (except some regions in central and southwest of China's mainland) reveal that the extreme 30-minute precipitation from the IMERG data does not follow the expectations based on the CC relationship.

For an in-depth analysis, we plotted the extreme 30-minute precipitations against temperatures in Fig. 9. This figure illustrates the scatter plots of extreme 30-minute precipitation versus different temperatures for each climate zone. There is no relationship between precipitation and temperature in the arid (first row) and plateau (third row) regions, resulting in regression lines approximately parallel to the horizontal axis. However, an upward rate with a lower slope than the CC rate is observed without any peak structure in continental and humid regions. It indicates that it is more likely that in these areas, a selected temperature variable may have less impact on scaling short-duration events compared to long-duration events. Unlike other climate zones over tropical region, the extreme precipitation-temperature relation is sensitive to a temperature variable; however, none of these temperature variables support a positive scaling of precipitation extremes over this region. Less impact of temperature on SF values reveals that the precipitation rate plays a more critical role in determining the scaling than the temperature variable at the 30-minute scale.

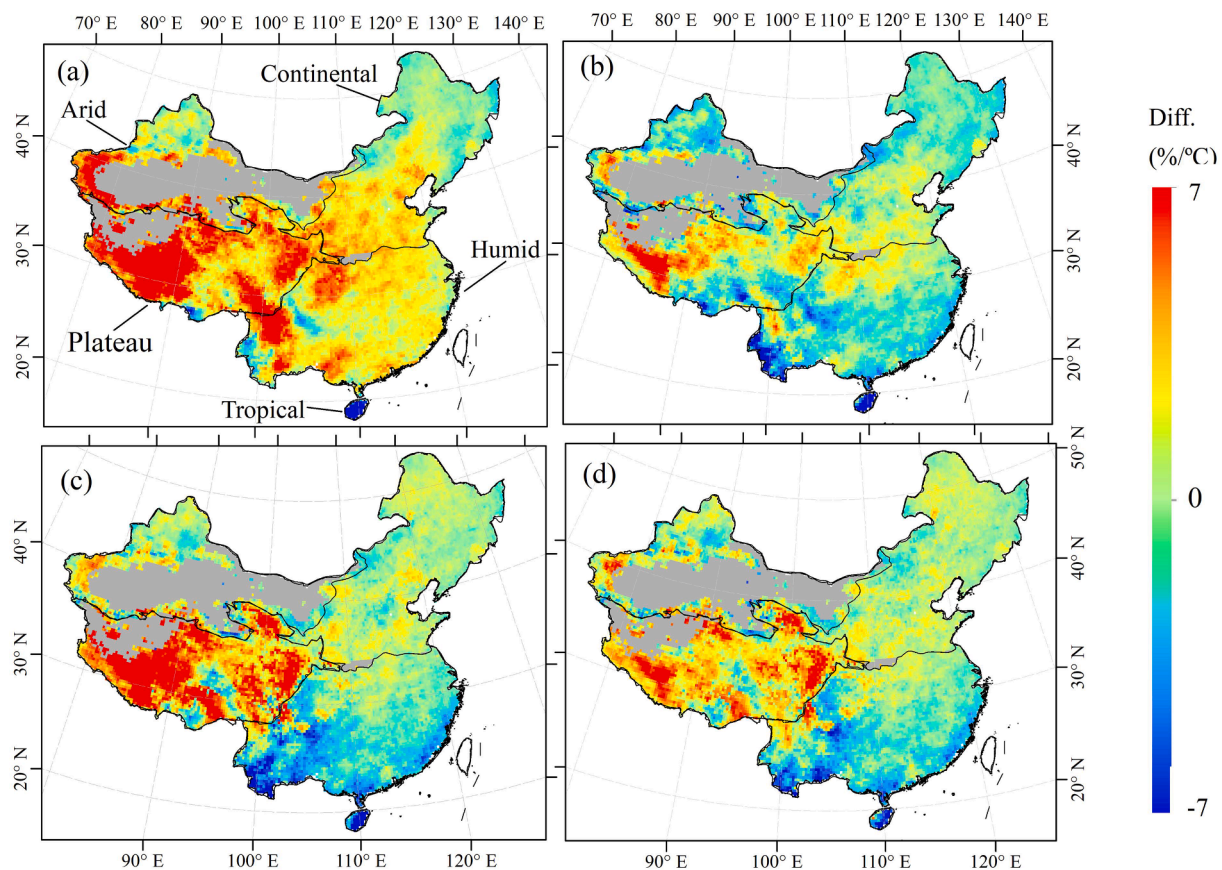


Fig. 6. The difference between calculated SFs for 99th percentile of daily precipitation of IMERG and CN05.1 datasets using (a) SAT, (b) DPT, (c) SAT-C, and (d) DPT-C over China's mainland. The polygons outlined by black lines represent five major climate zones in China's mainland. Positive values indicating that SFs of IMERG are larger than CN05.1 whereas the opposite is true for negative values. The gray areas represent the regions where SFs were not calculated due to lack of data. The IMERG results were upscaled to $0.25^{\circ} \times 0.25^{\circ}$ spatial resolution to match the CN05.1 resolution.

5. Discussion

5.1. Impact of different temperatures on scaling factor

According to the analysis above, our results at daily scale indicated that SF based on DTP with a more homogeneous spatial distribution is always positive across China's mainland, whereas the opposite is true for SAT (see Fig. 1). Negative SF values based on SAT have been widely reported in previous studies (e.g., Ali et al., 2018; Herath et al., 2018; Utsumi et al., 2011; Wang et al., 2017). In line with previous results reported for tropical regions of Australia (Bui et al., 2019; Wasko et al., 2018), a mixed negative and positive relationship between SAT and extreme daily precipitation were also found in tropical regions of China's mainland, while all SF values based on DPT are positive. Wasko et al. (2018) and Ali et al. (2018) also reported that SF values based on DPT are more uniform in space than those based on SAT. It is worth mentioning that despite the positive SF values in tropical area based on DPT, SAT-C, and DPT-C (see Fig. 1), the peak structure remains in some pixels (see Fig. 3). Indeed, during the heaviest rainfall in the tropical area, convective cloud cover and direct surface cooling by rainfall should reduce surface temperatures. At the same time, tropical storms and typhoons mix the upper overheated sea layer with colder waters of the thermocline, making the SAT lower than a few days before. All together, these processes promote the peak structure in the temperature-extreme rainfall relationship and “bend” linear scale factors.

In agreement with Visser et al. (2020), our results confirm that using temperature before the precipitation events, the SFs become positive based on SAT-C and DPT-C. Indeed, the cooling effect transfers heavy precipitation to the bins with lower temperatures (Bao et al., 2017).

Therefore, SAT-C and DPT-C may help better pairing precipitation and temperature resulted in heavy precipitations staying at the correct bins. However, at least over many regions of China's mainland, moisture limitation is the primary reason that controls heavy precipitation at higher temperatures, not the cooling effect and accompanying synoptic systems (Gao et al., 2020). It means that DPT and DPT-C are a potentially better proxy than SAT-C (and SAT) for scaling precipitation extremes. More specifically, we found that SFs from DPT are more consistent with the expected CC relation in arid, continental, and plateau regions, while DPT-C results in humid and tropical regions. It suggests that for scaling extreme daily precipitation over China's mainland, the relative humidity should be considered in all climate zones, while the cooling effect may not be critical in all regions. This can be explained by the fact that there would be more precipitation time in humid and tropical regions, and these precipitation events absorb considerable amounts of latent heat through precipitation evaporation. This finding is in line with Gao et al. (2020), who assessed the relationship between the extreme precipitations and within-day mean atmospheric temperature and antecedent maximum atmospheric temperature over China's mainland.

Our results indicate that a peak structure is present in the relationship between SAT and the extreme daily precipitation, with the SAT ranging from 17 to 24 °C across China's mainland. It suggests decreasing (daily) precipitation intensity with increasing temperatures (see Fig. 2). A similar temperature range was also reported over ten river basins in China by Wang et al. (2018). However, different breakpoints were reported for SAT-precipitation relationship over different regions, e.g., ~24 °C in South Korea (Park and Min, 2017), ~22 °C in the United Kingdom (Chen and Li, 2016), 20–26 °C in Australia (Hardwick Jones et al., 2010; Wasko et al., 2018), ~20 °C in the French Mediterranean

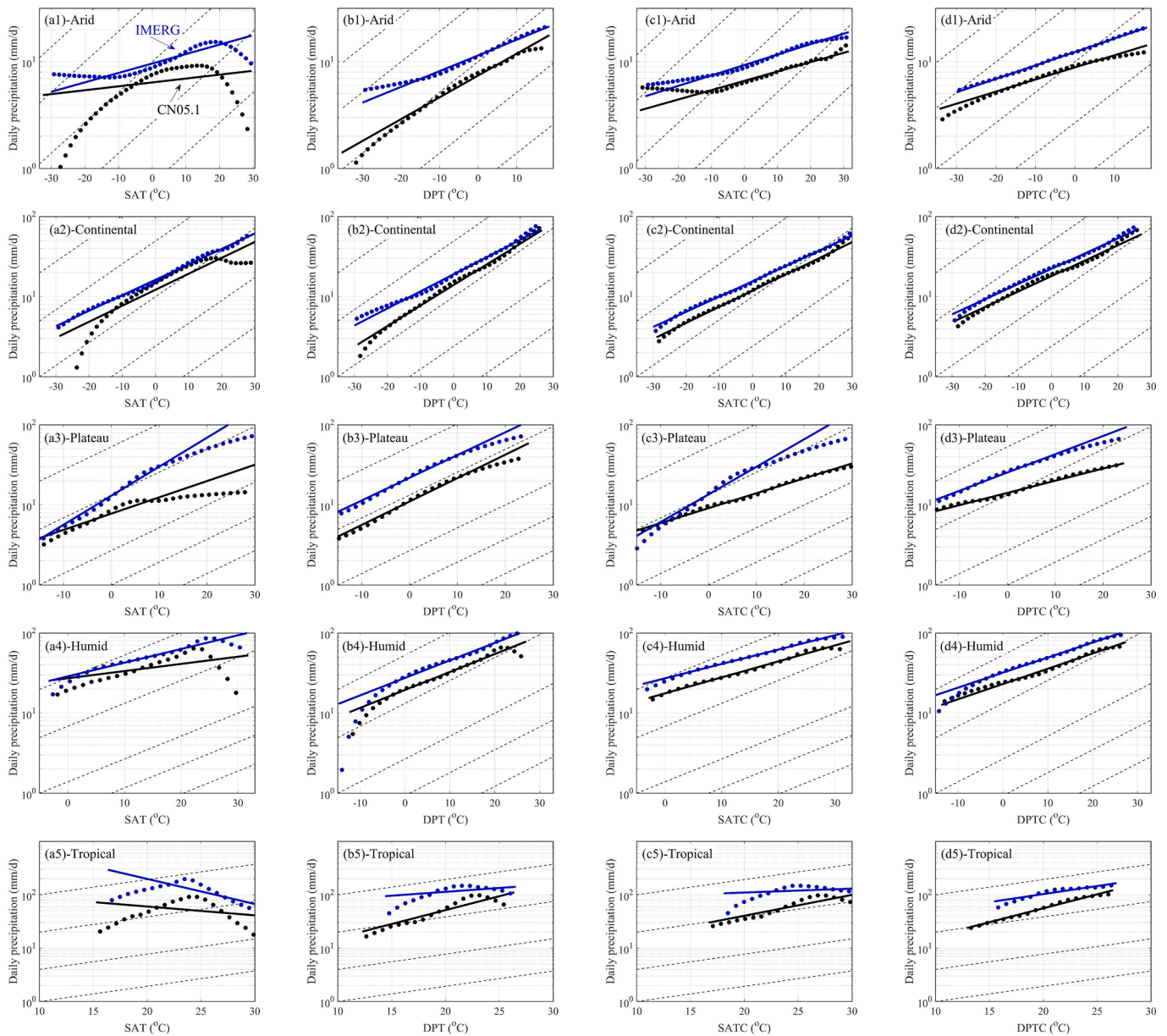


Fig. 7. The relationship between 99th percentile of daily precipitation of CN05.1 (black lines)/IMERG (blue lines) and (a) SAT, (b) DPT, (c) SAT-C, and (d) DPT-C in (1) arid, (2) continental, (3) plateau, (4) humid, and (5) tropical climate zones of China's mainland. The black dashed lines indicate CC like scaling of 6.8%/°C. The y-axis has a logarithmic scale. (For interpretation of the references to colour in this figure legend, the reader is referred to the web version of this article.)

area (Drobinski et al., 2016), ~ 18 °C in Romania (Busuioc et al., 2017). In many regions, precipitation is controlled by limited humidity at high temperatures (Berg et al., 2009; Herath et al., 2018). This limitation in relative humidity is more likely due to the moisture transport reduction from oceans to lands at high temperatures due to high humidity and a large saturation deficit over land (Gao et al., 2020). This implies that for temperature-precipitation relationship analysis, both moisture-holding capacity and available moisture should be considered (Hardwick Jones et al., 2010). Hence it could be expected that the peak structure may disappear when DPT/DPT-C is considered as the temperature indicator which takes into account relative humidity. However, our analysis cannot justify this expectation in all parts of China's mainland (see Fig. 3). It means that other factors than humidity play an important role e.g., rainfall duration (see Visser et al. (2021)). The peak structure in the relationship between extreme precipitation and DPT was also reported in the Netherlands (Zhang et al., 2017) and South Korea (Park and Min, 2017). Another issue that needs to be recalled is that SAT and

DPT represent surface temperature attributes, while both relative humidity and temperature significantly change with elevation i.e., the extreme precipitation largely associated with precipitable water within the air column (Roderick et al., 2020). Therefore, changes in rate of precipitation intensity with increasing temperature may not necessarily follow the CC relation. However, we showed the SFs calculated based on temperature range before the peak structure follow the CC scaling much better than the SFs obtained from a full temperature range (see Fig. 4). Indeed, it suggests that a single scaling rate could not be applied to interpret change in the daily extreme precipitation for all temperature range.

Although using DPT and DPT-C eliminates peak-like structures in some parts of China's mainland, remaining of peak structures in other parts induce uncertainty in estimating extreme precipitation under future global warming. The occurrence of peak structures contrasts with modeled precipitation extremes predictions and long-term trend analysis of annual maximum daily precipitation (Bao et al., 2017; Sun et al.,

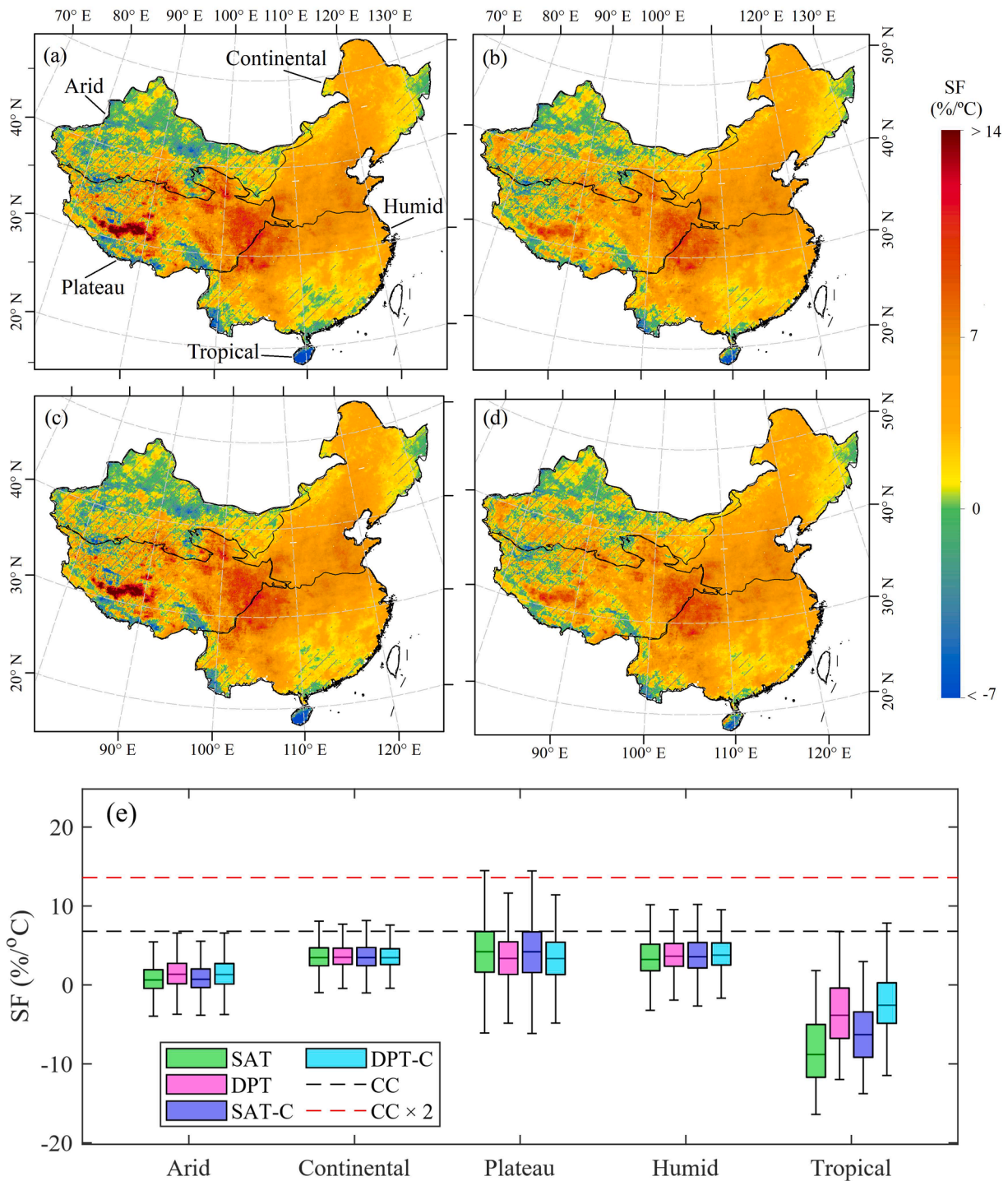


Fig. 8. Spatial distribution of SFs of 99th percentile of IMERG's 30-minute precipitations in relation with (a) SAT, (b) DPT, (c) SAT-C, and (d) DPT-C over China's mainland. The polygons outlined by black lines represent five major climate zones in China's mainland. The gray diagonal lines represent the regions without a statistically significant relationship between extreme precipitation and SAT/DPT/SAT-C/DPT-C at the 95% confidence level based on the *t*-test. SF greater than 14 %/°C and less than -7 %/°C was set as 14 %/°C and -7 %/°C, respectively. (e) Box plots show the SFs for five major climate zones of China's mainland. The bottom, middle, and top lines of each box are the 25th, 50th and 75th percentiles of SF, respectively, and whiskers are the 5th and 95th percentiles of SF. The dashed black and red lines indicate CC and super CC like scaling of 6.8 and 13.6 %/°C, respectively. (For interpretation of the references to colour in this figure legend, the reader is referred to the web version of this article.)

2020). Indeed, the binning curves for current and future warmer conditions are similar, except that the peak occurs at a higher temperature with more intense precipitation in the future (Zhang et al., 2017). Therefore, the binning scaling may not be reliable for use in projecting the impact of future warming on extreme precipitation. Under this circumstance, a trend scaling (Zhang et al., 2017) may provide a better

prediction, as Sun et al. (2020) discussed in detail.

Other studies indicated that SF based on DPT may not be as sensitive to storm duration (Wasko et al., 2018) and the type of precipitation event (Bui et al., 2019). However, the shape of the precipitation-temperature curve may be affected by the storm duration and precipitation type due to different dynamic processes. In fact, on a daily scale,

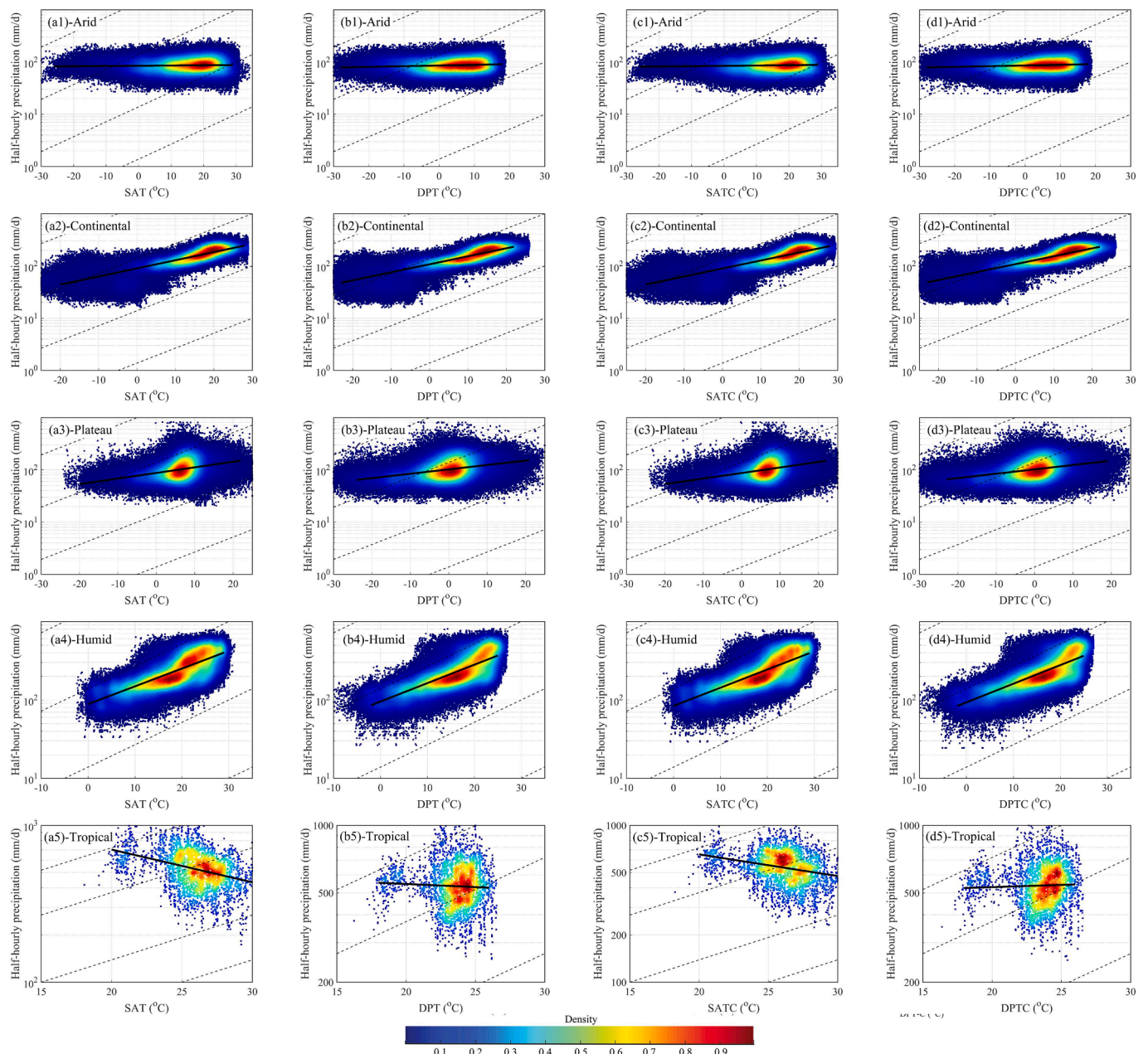


Fig. 9. The relationship between 99th percentile of IMERG’s 30-minute precipitations and (a) SAT, (b) DPT, (c) SAT-C, and (d) DPT-C in (1) arid, (2) continental, (3) plateau, (4) humid, and (5) tropical climate zones of China’s mainland. The solid black lines represent the 99th percentile lines fitted between extreme half-hourly precipitation and corresponding SAT/DPT/SAT-C/DPT-C. The dashed lines indicate CC like scaling of 6.8%/°C. Shaded colors indicate the probability density of the data based on a Gaussian kernel estimator. The y-axis has a logarithmic scale.

all precipitation events are considered regardless of their durations. Because duration of a single rainfall event decreases with increasing temperature (Gao et al., 2018), SF on a daily scale may not be valid in a warmer climate. In this regard, Visser et al. (2021) argued that the negative SFs over the Australia are due to decrease in the duration of the precipitation event at higher temperatures, and not to the decrease in the precipitation rate. Moreover, combining stratiform, convective, and mixed rainfall types may affect the scaling rate (Molnar et al., 2015) as a stronger increase in convective extremes rainfall was detected compared to the stratiform type rainfall (Berg et al., 2013). Due to these uncertainties, the relationship between precipitation extremes and temperature cannot be fully understood using the binning method (Zhang et al., 2017).

In addition, increasing number of short convective thunderstorms at

a high SAT (Westra et al., 2014) is the another reason for the extreme daily precipitation-temperature curve deviating from a monotonic curve. precipitation-temperature relation only explains the role of temperature in shaping precipitation through thermodynamic processes. Temperatures alone could not fully explain precipitation change. Estimating extreme precipitation requires both thermodynamic and dynamic processes (Jiang et al., 2020; Muller and Takayabu, 2020). However, the difference between the SF values based on different temperatures indicates that although there are some other influencing factors on precipitation extremes, a correct precipitation-temperatures sampling is essential in scaling precipitation extremes.

5.2. The performance of using IMERG in representing the extreme precipitation-temperature relationship

Our results indicated that IMERG estimates a larger amount of extreme daily precipitation than CN05.1 (see Fig. 7). This indicates a positive bias in IMERG data over China's mainland in all intensity classes of daily precipitation. This finding is consistent with the primary assessment of IMERG over China's mainland (e.g., Chen and Li, 2016; Tang et al., 2020). We found that the IMERG data can provide useful information about the effects of different temperatures on SF at a daily scale (see Fig. 5), while their effects are less notable on a 30-minute scale (see Fig. 8). We may have no (or smoother) peak structure at a sub-hourly time scale even when SAT is used, as Utsumi et al. (2011) reported, resulting in a closer SF value in different temperatures. In other words, the merits of accurate sampling on a coarser time scale are more evident (e.g., daily scale). However, due to some discrepancies with previous researches, the results at the 30-minute scale remain doubtful. Visser et al. (2020) showed that the difference between SFs calculated based on a dry-bulb and an antecedent dry-bulb temperature is significant at a sub-hourly scale. Moreover, our results show SF values at the 30-minute scale are smaller than ones at the daily scale. This is not consistent with previous findings that reported a higher SF value for a sub-daily scale compared to the daily ones (e.g., Ali et al., 2021; Lenderink et al., 2021; Lenderink and Van Meijgaard, 2008).

The root causes of the poorer performance of scaling precipitation extremes by using IMERG data at the 30-minute scale compared to the daily scale can be:

- The satellite sensors and IMERG algorithm have difficulty estimating the heavy rainfall (Fang et al., 2019; Mitra et al., 2018), i.e., it is more likely that the performance of IMERG is worse in estimating maximum 30-minute intensity;
- The IMERG data are adjusted at a monthly scale (Hosseini-Moghari and Tang, 2020); therefore, precipitation at the daily scale might be close to the observation, while the intensity of individual precipitation events with a high temporal resolution would not be adjusted well;
- The short precipitation events are hardly captured by satellites due to their limited numbers of overpasses and uneven sampling of the satellites (Gebregiorgis and Hossain, 2013; Tian et al., 2009).

It should be noted that it is better to compare IMERG 30-minute results with observed data. However, this paper does not make a quantitative assessment of IMERG at a 30-minute scale due to data availability issues. Therefore, at a 30-minute scale, we compared our results with previous studies and the CC relation.

The different temperatures have more impact on the extreme 30-minute precipitation in the tropical area, where these extremes are frequently associated with typhoons (see Fig. 9). At the same time, the worst performance of IMERG was reported exactly over this region, where SFs are negative based on all temperature variables (see Fig. 8). The reason for this mishap can be traced to heavy rainfall associated with tropical depressions, storms, and hurricanes (typhoons), as proper estimation of such rainfall events are difficult by IMERG (Omranian et al., 2018; Yu et al., 2021). It is worth mentioning that the poor performance of scaling precipitation extreme by using IMERG data at the 30-minute scale can also be related to the temperature data as we used daily temperature data for scaling the 30-minute precipitation.

6. Conclusions

In this study, the relationship between extreme daily/30-minute precipitation and temperature was explored throughout five climate zones of China's mainland. To this end, meteorological data from CN05.1 at the daily scale and precipitation data from IMERG datasets at the 30-minute scale were considered. Based on a comprehensive analysis

of grid-level climatic data, our results showed that:

A stronger relationship is found between extreme precipitation and daily DPT than SAT over China's mainland. There is a significant linear relationship between extreme precipitation and DPT in 98.5% of areas, whereas this value is 53.7% based on SAT. In ~ 62% areas, SF based on DPT is close to or excess of CC like scaling, i.e., 6 %/°C, while only ~ 18% areas have SF based on SAT over 6 %/°C. Moreover, SF based on DPT is always positive, whereas, in ~ 18% of areas, SF based on SAT is negative. The most substantial difference in SF values based on SAT and DPT was found in tropical regions where the median of the sensitivity of extreme precipitations to SAT and DPT is close to zero and 12.2 %/°C, respectively.

The cooling effect is a reason for negative SF based on SAT. If the antecedent SAT is used, all SF values turn to positive across all climatic zones. However, the SF based on SAT-C is lower than DPT. Our results based on DPT in arid, continental, and plateau lands and DPT-C in humid and tropical regions are more consistent with the expected CC relation compared to SAT-C because the peak structure in the precipitation and temperature relationship based on DPT and DPT-C is less evident. The cooling effect after precipitation and solar radiation blocking by heavy cloudiness in humid and tropical regions (in our study, these are the tropical islands in South China Sea surrounded by permanently warm waters and affected by frequent tropical storms/typhoons) is likely the reason for following better the expected CC relation by DPT-C in comparison to DPT in these regions.

SF rates calculated based on the temperature range before the peak are close to CC scaling based on all temperatures and in all regions (except tropical area). It suggests that the results of all temperatures are almost comparable in a limited range of temperatures. However, the variations of the extreme daily precipitation at higher temperatures based on different temperatures lead to a considerable disagreement between their SFs when the full temperature range is considered. Therefore, a single scaling rate cannot be considered for entire temperature range.

When analysing the use of within-day and antecedent temperatures for deriving SFs and the peak structure at the daily scale, IMERG shows almost similar results to CN05.1 in most cases except for tropical and plateau regions. However, extreme precipitations from IMERG at a 30-minute scale show no relationship with temperature in many parts of China's mainland. Moreover, SFs values based on IMERG at the 30-minute scale are smaller than the daily scale and are not sensitive to different temperature variables used. Therefore, our analysis of the IMERG data did not allow us linking precipitation extremes at the 30-minute scale with temperature over China's mainland.

With all improvements, the peak structure persists in precipitation-temperature relation at high temperatures. Therefore, for a more precise precipitation prediction, the consideration of both thermodynamic and dynamic processes is essential.

It should be noted that extrapolating the extreme precipitation under global warming using the historical relationship between extreme precipitation and temperature remains a challenge (Zhang et al., 2017). In addition, relying solely on temperature is not a perfect approach for estimating extreme precipitations. Therefore, for a better understanding of extreme precipitation changes, other factors like moisture source, changing atmospheric circulation patterns, and oceanic impact should be included in the calculations (Ali et al., 2018; Hardwick Jones et al., 2010). Indeed, a careful combination of model simulations and empirical approach based on observations is the best way forward to incorporate changes in extreme precipitation in decision makings such as estimating design hydrologic extremes (Sharma et al., 2021). Finally, it should be mentioned that the station network in western China's mountainous terrain is sparse, so the data in this area may not be considered as a reliable source for IMERG evaluations at fine spatial and temporal resolutions. Therefore, it is suggested to conduct a similar analysis at a sub-daily or sub-hourly scale when and where more observational data will be available.

Funding

This study was funded by National Natural Science Foundation of China (41730645), the Strategic Priority Research Program of Chinese Academy of Sciences (XDA20060402), and Chinese Academy of Sciences President's International Fellowship Initiative (2019VEA0019). Project 572,867 sponsored by the University of Maryland – College Park, USA provided support to Pavel Yakovlevich Groisman.

CRedit authorship contribution statement

Seyed-Mohammad Hosseini-Moghari: Conceptualization, Methodology, Data curation, Formal analysis, Investigation, Writing - original draft. **Siao Sun:** Writing - review & editing. **Qihong Tang:** Conceptualization, Methodology, Supervision, Writing - review & editing. **Pavel Yakovlevich Groisman:** Supervision, Writing - review & editing.

Declaration of Competing Interest

The authors declare that they have no known competing financial interests or personal relationships that could have appeared to influence the work reported in this paper.

Acknowledgments

We thank the National Climate Center of China Meteorological Administration and the National Aeronautics and Space Administration (NASA) for providing the CN05.1 and IMERG data, respectively. The CN05.1 product is available at the China Meteorological Data Service Center (CMDC; <http://data.cma.cn/>). The IMERG product is available through <https://disc.gsfc.nasa.gov/>.

Appendix A. Supplementary data

Supplementary data to this article can be found online at <https://doi.org/10.1016/j.jhydrol.2021.127391>.

References

- Ali, H., Fowler, H.J., Lenderink, G., Lewis, E., Pritchard, D., 2021. Consistent Large-Scale Response of Hourly Extreme Precipitation to Temperature Variation Over Land. *Geophys. Res. Lett.* 48, e2020GL090317. <https://doi.org/10.1029/2020GL090317>.
- Ali, H., Fowler, H.J., Mishra, V., 2018. Global observational evidence of strong linkage between dew point temperature and precipitation extremes. *Geophys. Res. Lett.* 45 (22), 12,320–12,330. <https://doi.org/10.1029/2017GL074917>.
- Ali, H., Mishra, V., 2017. Contrasting response of rainfall extremes to increase in surface air and dewpoint temperatures at urban locations in India. *Sci. Rep.* 7, 1228. <https://doi.org/10.1038/s41598-017-01306-1>.
- Sharma, A., Hettiarachchi, S., Wasko, C., 2021. Estimating design hydrologic extremes in a warming climate: alternatives, uncertainties and the way forward. *Philos. Trans. R. Soc. A* 379 (2195), 20190623. <https://doi.org/10.1098/rsta.2019.0623>.
- Bao, J., Sherwood, S.C., Alexander, L.V., Evans, J.P., 2017. Future increases in extreme precipitation exceed observed scaling rates. *Nat. Clim. Chang.* 7 (2), 128–132. <https://doi.org/10.1038/nclimate3201>.
- Barbero, R., Fowler, H.J., Blenkinsop, S., Westra, S., Moron, V., Lewis, E., Chan, S., Lenderink, G., Kendon, E., Guerreiro, S., Li, X.-F., Villalobos, R., Ali, H., Mishra, V., 2019. A synthesis of hourly and daily precipitation extremes in different climatic regions. *Weather Clim. Extrem.* 26, 100219. <https://doi.org/10.1016/j.wace.2019.100219>.
- Barbero, R., Fowler, H.J., Lenderink, G., Blenkinsop, S., 2017. Is the intensification of precipitation extremes with global warming better detected at hourly than daily resolutions? *Geophys. Res. Lett.* 44 (2), 974–983. <https://doi.org/10.1002/grl.v44.210.1002/2016GL071917>.
- Barenbrug, A.W.T., 1974. Psychrometry and psychrometric charts, 3rd ed. ed. Cape and Transvaal, Cape Town, S. Afr.
- Beck, H.E., Zimmermann, N.E., McVicar, T.R., Vergopolan, N., Berg, A., Wood, E.F., 2018. Present and future Köppen-Geiger climate classification maps at 1-km resolution. *Sci. Data* 5, 180214. <https://doi.org/10.1038/sdata.2018.214>.
- Berg, P., Haerter, J.O., Thejll, P., Piani, C., Hagemann, S., Christensen, J.H., 2009. Seasonal characteristics of the relationship between daily precipitation intensity and surface temperature. *J. Geophys. Res.* 114, D18102. <https://doi.org/10.1029/2009JD012008>.
- Berg, P., Moseley, C., Haerter, J.O., 2013. Strong increase in convective precipitation in response to higher temperatures. *Nat. Geosci.* 6 (3), 181–185. <https://doi.org/10.1038/ngeo1731>.
- Blenkinsop, S., Chan, S.C., Kendon, E.J., Roberts, N.M., Fowler, H.J., 2015. Temperature influences on intense UK hourly precipitation and dependency on large-scale circulation. *Environ. Res. Lett.* 10 (5), 054021. <https://doi.org/10.1088/1748-9326/10/5/054021>.
- Bui, A., Johnson, F., Wasko, C., 2019. The relationship of atmospheric air temperature and dew point temperature to extreme rainfall. *Environ. Res. Lett.* 14 (7), 074025. <https://doi.org/10.1088/1748-9326/ab2a26>.
- Busuoiuc, A., Baciu, M., Breza, T., Dumitrescu, A., Stoica, C., Baghina, N., 2017. Changes in intensity of high temporal resolution precipitation extremes in Romania: implications for Clausius-Clapeyron scaling. *Clim. Res.* 72 (3), 239–249. <https://doi.org/10.3354/cr01469>.
- Caloiero, T., Caroletti, G.N., Coscarelli, R., 2021. IMERG-Based Meteorological Drought Analysis over Italy. *Climate* 9, 65. <https://doi.org/10.3390/cli9040065>.
- Chen, F., Li, X., 2016. Evaluation of IMERG and TRMM 3B43 Monthly Precipitation Products over Mainland China. *Remote Sens.* 8, 472. <https://doi.org/10.3390/rs8060472>.
- Drobinski, P., Alonzo, B., Bastin, S., Silva, N.D., Muller, C., 2016. Scaling of precipitation extremes with temperature in the French Mediterranean region: What explains the hook shape? *J. Geophys. Res.* [Atmos.] 121 (7), 3100–3119. <https://doi.org/10.1002/jgrd.v121.710.1002/2015JD023497>.
- Escrig, H., Batlles, F.J., Alonso, J., Baena, F.M., Bosch, J.L., Salbidegoitia, I.B., Burgaleta, J.I., 2013. Cloud detection, classification and motion estimation using geostationary satellite imagery for cloud cover forecast. *Energy* 55, 853–859. <https://doi.org/10.1016/j.energy.2013.01.054>.
- Fang, J., Yang, W., Luan, Y., Du, J., Lin, A., Zhao, L., 2019. Evaluation of the TRMM 3B42 and GPM IMERG products for extreme precipitation analysis over China. *Atmos. Res.* 223, 24–38. <https://doi.org/10.1016/j.atmosres.2019.03.001>.
- Fowler, H.J., Ali, H., Allan, R.P., Ban, N., Barbero, R., Berg, P., Blenkinsop, S., Cabi, N.S., Chan, S., Dale, M., Dunn, R.J.H., Ekström, M., Evans, J.P., Fossier, G., Golding, B., Guerreiro, S.B., Hegerl, G.C., Kahraman, A., Kendon, E.J., Lenderink, G., Lewis, E., Li, X., O'Gorman, P.A., Orr, H.G., Peat, K.L., Prein, A.F., Pritchard, D., Schär, C., Sharma, A., Stott, P.A., Villalobos-Herrera, R., Villarini, G., Wasko, C., Wehner, M.F., Westra, S., Whitford, A., 2021. Towards advancing scientific knowledge of climate change impacts on short-duration rainfall extremes. *Philos. Trans. R. Soc. A Math. Phys. Eng. Sci.* 379 (2195), 20190542. <https://doi.org/10.1098/rsta.2019.0542>.
- Fujibe, F., 2013. Clausius-Clapeyron-like relationship in multidecadal changes of extreme short-term precipitation and temperature in Japan. *Atmos. Sci. Lett.* 14 (3), 127–132. <https://doi.org/10.1002/asl2.428>.
- Gao, X., Guo, M., Yang, Z., Zhu, Q., Xu, Z., Gao, K., 2020. Temperature dependence of extreme precipitation over mainland China. *J. Hydrol.* 583, 124595. <https://doi.org/10.1016/j.jhydrol.2020.124595>.
- Gao, X., Zhu, Q., Yang, Z., Liu, J., Wang, H., Shao, W., Huang, G., 2018. Temperature dependence of hourly, daily, and event-based precipitation extremes over China. *Sci. Rep.* 8, 17564. <https://doi.org/10.1038/s41598-018-35405-4>.
- Gebregiorgis, A.S., Hossain, F., 2013. Understanding the Dependence of Satellite Rainfall Uncertainty on Topography and Climate for Hydrologic Model Simulation. *IEEE Trans. Geosci. Remote Sens.* 51 (1), 704–718. <https://doi.org/10.1109/TGRS.2012.2196282>.
- Han, W., Liang, C., Jiang, B., Ma, W., Zhang, Y., 2016. Major natural disasters in China, 1985–2014: occurrence and damages. *Int. J. Environ. Res. Public Health* 13, 1118. <https://doi.org/10.3390/ijerph13111118>.
- Hardwick Jones, R., Westra, S., Sharma, A., 2010. Observed relationships between extreme sub-daily precipitation, surface temperature, and relative humidity. *Geophys. Res. Lett.* 37 (22), n/a–n/a. <https://doi.org/10.1029/2010GL045081>.
- Hegerl, G.C., Black, E., Allan, R.P., Ingram, W.J., Polson, D., Trenberth, K.E., Chadwick, R.S., Arkin, P.A., Sarojini, B.B., Becker, A., Dai, A., Durack, P.J., Easterling, D., Fowler, H.J., Kendon, E.J., Huffman, G.J., Liu, C., Marsh, R., New, M., Osborn, T.J., Skliris, N., Stott, P.A., Vidale, P.-L., Wijffels, S.E., Wilcox, L.J., Willett, K.M., Zhang, X., 2015. Challenges in quantifying changes in the global water cycle. *Bull. Am. Meteorol. Soc.* 96, 1097–1115. <https://doi.org/10.1175/BAMS-D-13-00212.1>.
- Held, I.M., Soden, B.J., 2006. Robust responses of the hydrological cycle to global warming. *J. Clim.* 19, 5686–5699. <https://doi.org/10.1175/JCLI3990.1>.
- Herath, S.M., Sarukkalgige, R., Nguyen, V.T.V., 2018. Evaluation of empirical relationships between extreme rainfall and daily maximum temperature in Australia. *J. Hydrol.* 556, 1171–1181. <https://doi.org/10.1016/j.jhydrol.2017.01.060>.
- Hosseini-Moghari, S.-M., Tang, Q., 2020. Validation of GPM IMERG V05 and V06 Precipitation Products over Iran. *J. Hydrometeorol.* 21, 1011–1037. <https://doi.org/10.1175/JHM-D-19-0269.1>.
- Huffman, G.J., Bolvin, D.T., Nelkin, E.J., 2015. Integrated Multi-satellite Retrievals for GPM (IMERG) technical documentation. NASA/GSFC Code 612, 47.
- Jiang, T., Su, B., Huang, J., Zhai, J., Xia, J., Tao, H., Wang, Y., Sun, H., Luo, Y., Zhang, L., Wang, G., Zhan, C., Xiong, M., Kundzewicz, Z.W., 2020. Each 0.5°C of Warming Increases Annual Flood Losses in China by More than US\$60 Billion. *Bull. Am. Meteorol. Soc.* 101, E1464–E1474. <https://doi.org/10.1175/BAMS-D-19-0182.1>.
- Roderick, T.P., Wasko, C., Sharma, A., 2020. An improved covariate for projecting future rainfall extremes? *Water Resour. Res.* 56 (8) <https://doi.org/10.1029/2019WR026924>.
- Köppen, W.P., 1936. Das Geographische System Der Klimate. W. Köppen, G. Geiger (Eds.), *Handbuch Der Klimatologie (Handbuch Der Klimatologie)*, vol. 1, C. Gebr. Borntraeger, Berlin (1936), p. 44.
- Lenderink, G., de Vries, H., Fowler, H.J., Barbero, R., van Ulft, B., van Meijgaard, E., 2021. Scaling and responses of extreme hourly precipitation in three climate

- experiments with a convection-permitting model. *Philos. Trans. R. Soc. A Math. Phys. Eng. Sci.* 379 (2195), 20190544. <https://doi.org/10.1098/rsta.2019.0544>.
- Lenderink, G., Mok, H.Y., Lee, T.C., van Oldenborgh, G.J., 2011. Scaling and trends of hourly precipitation extremes in two different climate zones – Hong Kong and the Netherlands. *Hydrol. Earth Syst. Sci.* 15 (9), 3033–3041. <https://doi.org/10.5194/hess-15-3033-201110.5194/hess-15-3033-2011-supplement>.
- Lenderink, G., van Meijgaard, E., 2008. Increase in hourly precipitation extremes beyond expectations from temperature changes. *Nat. Geosci.* 1, 511–514. <https://doi.org/10.1038/ngeo262>.
- Lenderink, G., Van Meijgaard, E., 2010. Linking increases in hourly precipitation extremes to atmospheric temperature and moisture changes. *Environ. Res. Lett.* 5, 25208. <https://doi.org/10.1088/1748-9326/5/2/025208>.
- Lewis, E., Fowler, H., Alexander, L., Dunn, R., McClean, F., Barbero, R., Guerreiro, S., Li, X.-F., Blenkinsop, S., 2019. GSDR: A Global Sub-Daily Rainfall Dataset. *J. Clim.* 32, 4715–4729. <https://doi.org/10.1175/JCLI-D-18-0143.1>.
- Li, X.-F., Blenkinsop, S., Barbero, R., Yu, J., Lewis, E., Lenderink, G., Guerreiro, S., Chan, S., Li, Y., Ali, H., Villalobos Herrera, R., Kendon, E., Fowler, H.J., 2020. Global distribution of the intensity and frequency of hourly precipitation and their responses to ENSO. *Clim. Dyn.* 54 (11–12), 4823–4839. <https://doi.org/10.1007/s00382-020-05258-7>.
- Li, S., Lei, Y., Zhang, Y., Liu, J., Shi, X., Hao, J., Chong, W., Chen, F., Chu, Q., 2019. Rational trade-offs between yield increase and fertilizer inputs are essential for sustainable intensification: A case study in wheat–maize cropping systems in China. *Sci. Total Environ.* 679, 328–336. <https://doi.org/10.1016/j.scitotenv.2019.05.085>.
- Mishra, V., Wallace, J.M., Lettenmaier, D.P., 2012. Relationship between hourly extreme precipitation and local air temperature in the United States. *Geophys. Res. Lett.* 39 (16), n/a–n/a. <https://doi.org/10.1029/2012GL052790>.
- Mitra, A.K., Kaushik, N., Kumar Singh, A., Parihar, S., Bhan, S.C., 2018. Evaluation of INSAT-3D satellite derived precipitation estimates for heavy rainfall events and its validation with gridded GPM (IMERG) rainfall dataset over the Indian region. *Remote Sens. Appl.: Soc. Environ.* 9, 91–99. <https://doi.org/10.1016/j.rsase.2017.12.006>.
- Molnar, P., Faticchi, S., Gaál, L., Szolgay, J., Burlando, P., 2015. Storm type effects on super Clausius-Clapeyron scaling of intense rainstorm properties with air temperature. *Hydrol. Earth Syst. Sci.* 19 (4), 1753–1766. <https://doi.org/10.5194/hess-19-1753-2015>.
- Muller, C., Takayabu, Y., 2020. Response of precipitation extremes to warming: what have we learned from theory and idealized cloud-resolving simulations, and what remains to be learned? *Environ. Res. Lett.* 15 (3), 035001. <https://doi.org/10.1088/1748-9326/ab7130>.
- Omrani, E., Sharif, H., Tavakoly, A., 2018. How Well Can Global Precipitation Measurement (GPM) Capture Hurricanes? Case Study: Hurricane Harvey. *Remote Sens.* 10, 1150. <https://doi.org/10.3390/rs10071150>.
- Panthou, G., Mailhot, A., Laurence, E., Talbot, G., 2014. Relationship between surface temperature and extreme rainfalls: a multi-time-scale and event-based analysis. *J. Hydrometeorol.* 15, 1999–2011. <https://doi.org/10.1175/JHM-D-14-0020.1>.
- Park, I.-H., Min, S.-K., 2017. Role of convective precipitation in the relationship between subdaily extreme precipitation and temperature. *J. Clim.* 30 (23), 9527–9537. <https://doi.org/10.1175/JCLI-D-17-0075.1>.
- Peel, M.C., Finlayson, B.L., McMahon, T.A., 2007. Updated world map of the Köppen-Geiger climate classification. *Hydrol. Earth Syst. Sci.* 11 (5), 1633–1644. <https://doi.org/10.5194/hess-11-1633-2007>.
- Schroeder, K., Kirchengast, G., 2018. Sensitivity of extreme precipitation to temperature: the variability of scaling factors from a regional to local perspective. *Clim. Dyn.* 50 (11–12), 3981–3994. <https://doi.org/10.1007/s00382-017-3857-9>.
- Sun, Q., Zwiers, F., Zhang, X., Li, G., 2020. A comparison of intra-annual and long-term trend scaling of extreme precipitation with temperature in a large-ensemble regional climate simulation. *J. Clim.* 33, 9233–9245. <https://doi.org/10.1175/JCLI-D-19-0920.1>.
- Tang, G., Clark, M.P., Papalexiou, S.M., Ma, Z., Hong, Y., 2020. Have satellite precipitation products improved over last two decades? A comprehensive comparison of GPM IMERG with nine satellite and reanalysis datasets. *Remote Sens. Environ.* 240, 111697. <https://doi.org/10.1016/j.rse.2020.111697>.
- Tang, Q., 2020. Global change hydrology: Terrestrial water cycle and global change. *Sci. China Earth Sci.* 63 (3), 459–462. <https://doi.org/10.1007/s11430-019-9559-9>.
- Tian, Y., Peters-Lidard, C.D., Eylander, J.B., Joyce, R.J., Huffman, G.J., Adler, R.F., Hsu, K., Turk, F.J., Garcia, M., Zeng, J., 2009. Component analysis of errors in satellite-based precipitation estimates. *J. Geophys. Res.* 114, D24101. <https://doi.org/10.1029/2009JD011949>.
- Trenberth, K.E., Dai, A., Rasmussen, R.M., Parsons, D.B., 2003. The Changing Character of Precipitation. *Bull. Am. Meteorol. Soc.* 84, 1205–1218. <https://doi.org/10.1175/BAMS-84-9-1205>.
- Trenberth, K.E., Zhang, Y., Gehne, M., 2017. Intermittency in Precipitation: Duration, Frequency, Intensity, and Amounts Using Hourly Data. *J. Hydrometeorol.* 18, 1393–1412. <https://doi.org/10.1175/JHM-D-16-0263.1>.
- Utsumi, N., Seto, S., Kanae, S., Maeda, E.E., Oki, T., 2011. Does higher surface temperature intensify extreme precipitation? *Geophys. Res. Lett.* 38 (16), n/a–n/a. <https://doi.org/10.1029/2011GL048426>.
- Visser, J.B., Wasko, C., Sharma, A., Nathan, R., 2020. Resolving Inconsistencies in Extreme Precipitation-Temperature Sensitivities. *Geophys. Res. Lett.* 47, e2020GL08972310.1029/2020GL089723.
- Visser, J. B., Wasko, C., Sharma, A., & Nathan, R., 2021. Eliminating the “hook” in Precipitation-Temperature Scaling. *J. Clim.* 1–42. <https://doi.org/10.1175/JCLI-D-21-0292.1>.
- Wang, G., Wang, D., Trenberth, K.E., Erfanian, A., Yu, M., Bosilovich, M.G., Parr, D.T., 2017. The peak structure and future changes of the relationships between extreme precipitation and temperature. *Nat. Clim. Chang.* 7, 268–274. <https://doi.org/10.1038/nclimate3239>.
- Wang, H., Sun, F., Liu, W., 2018. The dependence of daily and hourly precipitation extremes on temperature and atmospheric humidity over China. *J. Clim.* 31 (21), 8931–8944. <https://doi.org/10.1175/JCLI-D-18-0050.1>.
- Wasko, C., Lu, W.T., Mehrotra, R., 2018. Relationship of extreme precipitation, dry-bulb temperature, and dew point temperature across Australia. *Environ. Res. Lett.* 13 (7), 074031. <https://doi.org/10.1088/1748-9326/aad135>.
- Wasko, C., Sharma, A., 2015. Steeper temporal distribution of rain intensity at higher temperatures within Australian storms. *Nat. Geosci.* 8 (7), 527–529. <https://doi.org/10.1038/ngeo2456>.
- Wasko, C., Parinussa, R.M., Sharma, A., 2016. A quasi-global assessment of changes in remotely sensed rainfall extremes with temperature. *Geophys. Res. Lett.* 43 (24), 12–659. <https://doi.org/10.1002/2016GL071354>.
- Westra, S., Fowler, H.J., Evans, J.P., Alexander, L.V., Berg, P., Johnson, F., Kendon, E.J., Lenderink, G., Roberts, N.M., 2014. Future changes to the intensity and frequency of short-duration extreme rainfall. *Rev. Geophys.* 52 (3), 522–555. <https://doi.org/10.1002/2014RG000464>.
- Wibig, J., Piotrowski, P., 2018. Impact of the air temperature and atmospheric circulation on extreme precipitation in Poland. *Int. J. Climatol.* 38 (12), 4533–4549. <https://doi.org/10.1002/joc.5685>.
- Wu, J., Gao, X.J., 2013. A gridded daily observation dataset over China region and comparison with the other datasets, Chinese. *J. Geophys.* 56, 1102–1111. <https://doi.org/10.6038/cjg20130406>.
- Yang, Y., Tang, J., Xiong, Z., Dong, X., 2017. Evaluation of high-resolution gridded precipitation data in arid and semiarid regions: Heihe River Basin, Northwest China. *J. Hydrometeorol.* 18, 3075–3101. <https://doi.org/10.1175/JHM-D-16-0252.1>.
- Yin, J., Guo, S., Gentile, P., Sullivan, S.C., Gu, L., He, S., Chen, J., Liu, P., 2021. Does the Hook Structure Constrain Future Flood Intensification Under Anthropogenic Climate Warming? *Water Resour. Res.* 57, e2020WR02849110.1029/2020WR028491.
- Yong, Z., Xiong, J., Wang, Z., Cheng, W., Yang, J., Pang, Q., 2021. Relationship of extreme precipitation, surface air temperature, and dew point temperature across the Tibetan Plateau. *Clim. Change* 165, 41. <https://doi.org/10.1007/s10584-021-03076-2>.
- Yu, C., Hu, D., Di, Y., Wang, Y., 2021. Performance evaluation of IMERG precipitation products during typhoon Lekima (2019). *J. Hydrol.* 597, 126307. <https://doi.org/10.1016/j.jhydrol.2021.126307>.
- Zhang, X., Zwiers, F.W., Li, G., Wan, H., Cannon, A.J., 2017. Complexity in estimating past and future extreme short-duration rainfall. *Nat. Geosci.* 10 (4), 255–259. <https://doi.org/10.1038/ngeo2911>.
- Zhang, W., Villarini, G., Wehner, M., 2019. Contrasting the responses of extreme precipitation to changes in surface air and dew point temperatures. *Clim. Change* 154 (1), 257–271. <https://doi.org/10.1007/s10584-019-02415-8>.